Multi-objective Distributed Optimal Control for Photovoltaic-integrated Distribution Networks

Li Ma, Yifan Pang, Xin Liu, Zirui Li, Di Xiao, Qianqian Feng, Zhikui Yue

Abstract — **With the increasing penetration of distributed photovoltaics (PV) in distribution networks, rational control of PV-integrated distribution networks is crucial for ensuring their stable and economical operation. This paper proposes a multi-objective distributed optimal control for PV-integrated distribution networks. Firstly, three novel indexes are introduced: an improved electrical distance index, an intra-region autonomous regulation capability index, and an intra-region coupling strength index. Based on these indexes, an improved modularity index is proposed to partition PV-integrated distribution networks. Secondly, based on the partitioned distribution network, a multi-objective distributed optimal control model for distribution networks is formulated, aiming to minimize voltage violation magnitude, network losses, and PV inverter losses. An improved Alternating Direction Method of Multipliers (ADMM) is proposed to enhance solving efficiency by adjusting the penalty factor. Finally, case studies are conducted on the modified IEEE33 node system with distributed PV in MATLAB. Simulation results demonstrate that the partitioning method proposed in this paper significantly enhances the modularity index value, thereby achieving rational partitioning of the distribution network. Furthermore, the multi-objective distributed optimal control effectively mitigates voltage violations, reduces network losses and inverter losses, and improves computational efficiency, ultimately enhancing grid stability and economic performance.**

Index Terms—**Multi-objective, Distributed photovoltaics, Distribution network partition, Distributed optimal control, Improved ADMM**

I. Introduction

The growing penetration of distributed photovoltaics (PV) in distribution networks provides abundant control resources for voltage regulation. However, the integration of large-scale PV inverters also poses significant challenges to the economic operation of distribution networks[1]. In this context, rational control of PV-integrated distribution networks is crucial for ensuring their stable and economical operation. Voltage limit violations can lead to equipment overload, insulation aging, and even faults, directly compromising power supply reliability. Therefore, minimizing voltage violation magnitudes is critical for grid security[2]. Reducing network losses improves energy transmission efficiency, while minimizing inverter losses extends equipment lifespan and lowers maintenance costs, both of which are vital for economic operation[3]. Traditional centralized control methods struggle to adapt to the distributed nature and rapid response requirements of PV systems, and single-objective optimization may degrade other performance indexes[4]. Thus, developing a multi-objective distributed optimal control framework to minimize voltage violation magnitude, network losses and inverter losses is of significant practical relevance[5].

Current approaches for optimal control of PV-integrated distribution networks can be categorized into three types: local optimal control, centralized optimal control, and distributed optimal control. Local and centralized methods are suitable for distribution networks with low PV penetration. However, as large-scale distributed PV systems are integrated, requiring control of numerous nodes and handling increasingly complex optimization variables, distributed optimal control has gained prominence in high-PV-penetration networks. Reference [6] proposed a hierarchical distributed control method with autonomous-collaborative mode switching for microgrids. By dynamically establishing or disconnecting communication links between microgrids, this method enables voltage regulation across microgrids and common buses while supporting autonomous or collaborative operation. Reference [7] established a partitioned distributed voltage optimization model targeting PV active power curtailment and network loss minimization. Through reformulation of the augmented Lagrangian function, global optimization was achieved via the Alternating Direction Method of Multipliers (ADMM). Reference [8] identified critical nodes within partitioned distribution networks and applied a modified particle swarm optimization algorithm to minimize network losses and voltage fluctuations by regulating these nodes. Although these studies advanced voltage control methodologies, they overlooked PV inverter losses, potentially leading to suboptimal solutions and increased operational costs. To address these gaps, this paper proposes a multi-objective distributed optimal control framework that jointly minimizes voltage violation magnitudes, network losses, and PV inverter losses. This approach ensures both secure and economic operation under

Manuscript received April 23, 2025; revised August 9, 2025.

Li Ma is a postgraduate tutor in the Department of Electrical and Control Engineering at Xi'an University of Science and Technology, Xi'an, 710699, P. R. China (e-mail: 710849937@qq.com).

Yifan Pang is a postgraduate student in the Department of Electrical and Control Engineering at Xi'an University of Science and Technology, Xi'an, 710699, P. R. China (Corresponding author, e-mail: 1261587641@qq.com).

Xin Liu is a technician in the Grid Sichuan Electric Power Company Neijiang Power Supply Company, Neijiang, 641003, P. R. China (e-mail: 1083534364@qq.com).

Zirui Li is a postgraduate student in the Department of Electrical and Control Engineering at Xi'an University of Science and Technology, Xi'an, 710699, P. R. China (e-mail: 1030848936@qq.com).

Di Xiao is a postgraduate student in the Department of Electrical and Control Engineering at Xi'an University of Science and Technology, Xi'an, 710699, P. R. China (e-mail: 2679900617@qq.com).

Qianqian Feng is a postgraduate student in the Department of Electrical and Control Engineering at Xi'an University of Science and Technology, Xi'an, 710699, P. R. China (e-mail: 2596490641@qq.com).

Zhikui Yue is a postgraduate student in the Department of Electrical and Control Engineering at Xi'an University of Science and Technology, Xi'an, 710699, P. R. China. (e-mail: 1402729326@qq.com).

high PV penetration.

The partitioning management strategy for distributed PV-integrated distribution networks enhances the coordination of PV resource allocation, optimizes local energy consumption, and ensures intra-partition and inter-partition collaboration[9]. Due to the distributed and decentralized nature of PV systems, selecting appropriate partitioning indexes is critical during grid planning and dispatch[10]. Reference [11] introduced an electrical distance index based on active power-phase angle sensitivity. By calculating intra-partition and inter-partition electrical distances, the network is clustered into manageable zones. Reference [12] proposed an improved modularity index incorporating network topology, power flow, and voltage management measures. This approach achieves global voltage regulation by controlling voltage profiles within sub-communities. Reference [13] developed a structural electrical distance index that jointly considers active and reactive power outputs to delineate voltage regulation zones for distributed energy resources. While these studies advanced partitioning indexes, their applicability is limited to structurally simple grids with low PV penetration. Large-scale PV integration complicates grid topology and intensifies optimization challenges. Thus, this paper proposes a high-PV-penetration-adapted modularity index that enables coordinated control across partitions, significantly improving grid optimization efficiency.

This paper focuses on distribution networks with integrated distributed PV and proposes a multi-objective distributed optimal control for PV-integrated distribution networks. The structure of the paper is organized as follows: Section 2 investigates the partitioning methodology for PV-integrated distribution networks. The improved modularity index proposed in this work is solved using the Louvain algorithm to achieve network partitioning tailored for high-PV-penetration scenarios. Section 3 presents the partition-based distributed optimal control framework, aiming to maximally mitigate voltage violations while minimizing network losses and inverter losses. To accelerate convergence, an improved ADMM is proposed to coordinate optimization across partitions. Section 4 validates the proposed method through simulations on a modified IEEE33 node system. The results demonstrate that the multi-objective distributed optimal control not only effectively alleviates voltage violations but also minimizes network losses and PV inverter losses during optimization. Additionally, the framework achieves global optimal control by fully leveraging the regulation capabilities of dispatchable resources, ensuring both grid stability and economic efficiency. Section 5 gives the conclusion.

II. Research on Partitioning Methods for PV-integrated Distribution Networks

A. Partitioning Indexes for PV-integrated Distribution Networks

With the increasing integration of distributed PV into distribution networks, system control complexity intensifies, necessitating rational partitioning of the distribution network to achieve coordinated control.

1) Improved Electrical Distance Index

The voltage/power sensitivity between nodes can be derived from the inverse of the Jacobian matrix in power flow calculations. Based on the AC power flow equations, the nonlinear power flow equations are linearized at the steady-state solution, yielding the matrix expression:

$$\begin{bmatrix}\Delta\theta\\ \Delta U\end{bmatrix}=\begin{bmatrix}S_{P\theta} & S_{Q\theta}\\ S_{PU} & S_{QU}\end{bmatrix}\begin{bmatrix}\Delta P\\ \Delta Q\end{bmatrix} \tag{1}$$

Where S_{PU} and S_{QU} are the sensitivity coefficients of active and reactive power injections at node *j* to the voltage magnitude at node *i*, respectively; $S_{P\theta}$ and $S_{Q\theta}$ are the sensitivity coefficients of active and reactive power injections at node *j* to the voltage phase angle at node *i*, respectively.

During steady-state operation, the primary factor influencing voltage magnitude is reactive power. As shown in (1), the relationship between node voltage and reactive power variations in the distribution network can be expressed as:

$$\Delta U = S_{QU}\Delta Q \tag{2}$$

When defining the electrical distance, considering only the physical positions of nodes in the distribution network is insufficient. Specifically, if a node has few adjacent edges but its neighboring nodes have numerous edges, voltage violations at adjacent nodes may still propagate to it, meaning the node remains vulnerable to voltage violations from others[14]. Therefore, this paper proposes an improved electrical distance index that comprehensively incorporates information from both the node and its adjacent nodes:

$$e_{ij}^{QU} = S_{ij}^{QU} + \sum_{d\in D} S_{dj}^{QU} \tag{3}$$

where *d* represents an adjacent node of node *i*; *D* is the set of adjacent nodes of node *i*.

2) Intra-region Autonomous Regulation Capability Index

This paper introduces the intra-region autonomous regulation capability index to balance voltage regulation resources within each partition. This ensures that PV output and load demand within each partition are locally balanced, avoiding long-distance power transmission, reducing transmission losses, alleviating system regulation burdens, and ultimately enhancing grid stability. The proposed index is formulated as:

$$F_{c_k}=\begin{cases}\dfrac{Q_{c_k}^{\sup}-Q_{c_k}^{need}}{Q_{c_k}^{avg}} & , \ Q_{c_k}^{avg}\geq Q_{c_k}^{\sup}-Q_{c_k}^{need}\\ 1 & ,otherwise\end{cases} \tag{4}$$

Where c_k denotes the *k*-th partition; F_{c_k} represents the intra-region autonomous regulation capability index of the *k*-th partition; $Q_{c_k}^{\sup}$、$Q_{c_k}^{need}$ corresponds to the reactive power supply capacity and demand value of the *k*-th partition, respectively; $Q_{c_k}^{avg}$ is the average reactive power supply value of the *k*-th partition. The intra-region autonomous regulation capability index F_{c_k} reflects the regulation difficulty of the distribution network. A smaller F_{c_k} indicates that reactive power fluctuations within the partition are closer to the average value, implying moderate dependence on external power supply variations and easier

load-generation balance. Conversely, a larger F_{c_k} signifies greater regulation difficulty, necessitating additional flexible regulation resources to ensure power supply-demand equilibrium.

3) Intra-region Coupling Strength Index

The modularity function measures the structural strength of a specific partition in a network and is a critical index in clustering algorithms. The traditional modularity function is defined as:

$$\rho=\frac{1}{2m}\sum_i\sum_j\left[A_{ij}-\chi\frac{k_i k_j}{2m}\right]\delta(i,j) \tag{5}$$

Where A_{ij} is the edge weight between nodes *i* and *j*; k_i is the sum of edge weights connected to node *i*; k_j is the sum of edge weights connected to node *j*; $m=\left(\sum_i\sum_j A_{ij}\right)/2$ is the total sum of all edge weights in the network; $\delta(i,j)=1$ when nodes *i* and *j* belong to the same partition, otherwise $\delta(i,j)=0$; χ is the resolution parameter in the modularity function, set to $\chi=1$. This paper employs the average edge weight to represent the partition weight, which quantifies the coupling strength between two nodes:

$$A_{ij}=\frac{e_{ij}^{QU}+e_{ji}^{QU}}{2} \tag{6}$$

This paper proposes an intra-region coupling strength index to quantify the coupling intensity among partitions. This index balances the number of nodes and PV integrations within each partition, preventing unreasonable partitioning. The proposed index is formulated as:

$$\beta_{c_k}^{QU}=\frac{2\sum_{i.j=1}^{n}A_{ij}^{Q}}{n(n-1)} \tag{7}$$

Where *n* is the number of nodes in the partition c_k, and theoretically, these nodes can form up to *n*(*n*-1)/2 edges. A higher intra-region coupling strength index indicates stronger coupling within the partition.

4) Improved Modularity Index

The sensitivity between nodes in a distribution network is related to their equivalent reactance parameters, while impedance characteristics are directly influenced by the spatial distribution of nodes[15]. Constructing partition weights based on the voltage-reactive power sensitivity matrix ensures continuity of power transmission and electrical coupling strength between partitions[16]. Combining (5) and (6), the partition modularity index is derived as:

$$\rho_{QU}=\frac{1}{2m}\sum_i\sum_j\left[A_{ij}-\frac{k_i k_j}{2m}\right]\delta(i,j) \tag{8}$$

Assuming the distribution network is divided into N partitions, the improved modularity index is expressed as:

$$\rho_{imp}=\rho_{QU}+\frac{1}{N}\left(\left(1-F_{c_k}\right)+\beta_{c_k}^{QU}\right) \tag{9}$$

The proposed improved modularity index not only incorporates node location information but also balances reactive power supply and load demand within each partition, preventing irrational partitioning caused by imbalanced load nodes and PV integrations.

B. Partitioning Algorithm for PV-integrated Distribution Networks

The Louvain algorithm can rapidly and automatically determine the optimal number of partitions without predefined assumptions, significantly reducing human intervention[17]. Its core principle involves iteratively optimizing the network modularity through local adjustments of node assignments, ultimately achieving effective partitioning. The steps for implementing the Louvain algorithm are as follows:

Step 1: Obtain operational data of the PV-integrated distribution network at the partitioning time.

Step 2: Initialize each node as an independent partition and calculate the $\rho_{imp,i}^{0}$ value using (9).

Step 3: Randomly select two nodes i and j to form a new partition (i,j). Calculate the value of $\rho_{imp,ij}^{1}$ and $\Delta\rho_1=\rho_{imp,ij}^{1}-\rho_{imp,i}^{0}$. Merge the node (i,j) corresponding to the maximum $\Delta\rho_1$ into a new partition.

Step 4: Treat the merged partition (i,j) as a new independent node. Rebuild the network and repeat Step 3 to continue partitioning.

Step 5: Iterate Steps 3-4 until all nodes are merged. Select the partition result with the maximum ρ_{imp}^{ij} value as the optimal solution.

The proposed improved modularity index incorporates node location information, enabling a dynamic partitioning mechanism with real-time responsiveness. This mechanism adaptively handles operational changes such as PV grid-connection state transitions and load fluctuations. For distribution networks, changes in topology or operational modes directly affect partitioning results. Retaining outdated partitions under such changes degrades control effectiveness. To ensure stability, partition updates are triggered only when topology-altering operational shifts occur.

III. Multi-objective Distributed Optimal Control for PV-integrated Distribution Networks

A. Multi-objective Distributed Optimal Control Model for PV-integrated Distribution Networks

Adopting optimization-based control methods to actively manage distributed PV systems and other grid voltage regulation devices can effectively mitigate voltage limit violations while enhancing economic benefits such as reduced network losses and inverter losses.

When PV systems perform reactive power regulation through inverters, a portion of electrical energy is consumed and converted into heat. This heat generation translates to reactive power losses. As the number of grid-connected distributed PV systems increases, excessive reactive power usage may escalate these losses. Furthermore, as highlighted in [18], the reactive power injection from proliferating distributed PV systems leads to non-negligible inverter losses. To accurately characterize inverter loss behavior, the study models inverter losses as a quadratic function of

inverter power output, approximating the power loss in inverters as Q_G^2.

Taking c_k as an example, this paper establishes a distributed optimal control model for the distribution network, with the optimization objectives of minimizing voltage violation magnitudes, network losses, and PV inverter losses. The model is formulated as follows:

$$\min f = \alpha f_1 + \beta f_2 \tag{10}$$

$$f_1 = \sum_{j\in c_k, \forall i: i\to j} r_{ij} l_{ij}^2 + Q_G^2 \tag{11}$$

$$f_2 = \sum_{i\in c_k} \left|1 - U_i\right| \tag{12}$$

Where f is the objective function of the autonomous optimization model for partition c_k; r_{ij} is the resistance value between nodes i and j; l_{ij} is the current flowing from node i into branch ij; $i:i\to j$ represents the upstream measurement node of node j; U_i is the voltage magnitude at node i; Q_G^2 is the inverter loss; α、β is the weighting factor for the objective functions. The weighting factors are determined based on the priorities assigned to each objective function by system operators and their operational experience. To ensure safe, stable, and efficient operation of the distribution network, power flows must be reasonably constrained and controlled. The constraints are as follows:

$$\sum_{i:i\to j}\left(P_{ij} - r_{ij} l_{ij}\right) - P_j = \sum_{l:j\to l} P_{jl} \tag{13}$$

$$\sum_{i:i\to j}\left(Q_{ij} - x_{ij} l_{ij}\right) - Q_j = \sum_{l:j\to l} Q_{jl} \tag{14}$$

$$v_j = v_i - 2\left(r_{ij}P_{ij} + x_{ij}Q_{ij}\right) + \left(r_{ij}^2 + x_{ij}^2\right) l_{ij} \tag{15}$$

$$l_{ij} = I_{ij}^2 = \frac{P_{ij}^2 + Q_{ij}^2}{v_i} \tag{16}$$

$$\begin{cases} P_j = P_{L,j} - P_{G,j} \\ Q_j = Q_{L,j} - Q_{G,j} - Q_{SVC,j} \end{cases} \tag{17}$$

$$\underline{V_j} \le V_j \le \overline{V_j} \tag{18}$$

$$\begin{cases} 0 \le P_{PV,n} \le \overline{P_{PV,n}} \\ \left|Q_{PV,n}^2\right| \le \sqrt{S_{PV,n}^2 - P_{PV,n}^2} \\ -P_{PV,n}\sqrt{1-k_f^2}/k_f \le Q_{PV,n} \le P_{PV,n}\sqrt{1-k_f^2}/k_f \end{cases} \tag{19}$$

$$\underline{Q_{SVC,j}} \le Q_{SVC,j} \le \overline{Q_{SVC,j}} \tag{20}$$

$$\left\| \begin{matrix} 2P_{ij} \\ 2Q_{ij} \\ l_{ij} - v_i \end{matrix} \right\|_2 \le l_{ij} + v_i \tag{21}$$

Where P_{ij} and Q_{ij} represent the active power and reactive power flowing from node i to branch ij, respectively; P_j and Q_j are the net active load and reactive load injected into node j; v_i and v_j are the squares of the voltage magnitudes at nodes i and j, respectively; x_{ij} is the reactance of branch ij; $P_{L,j}$ and $Q_{L,j}$ are the active power and reactive power of the load at node j; $P_{G,j}$ and $Q_{G,j}$ denote the actual active power output and reactive power output of the PV system at node j; $Q_{SVC,j}$ is the reactive power output of the Static Var Compensator (SVC); $\underline{V_j}$ and $\overline{V_j}$ are the lower and upper safety limits of the node voltage; k_f is the minimum power factor, set to 0.95; $\underline{Q_{SVC,j}}$ and $\overline{Q_{SVC,j}}$ are the lower and upper limits of the reactive power output of SVC.

B. Multi-objective Distributed Optimal Control Based on the ADMM

The ADMM offers significant advantages in solving modern optimization problems arising from big data and artificial intelligence[19]. Even when component functions are nonsmooth, the subproblems in ADMM can often be efficiently solved through coordinated iterations, enabling rapid convergence to the global optimal solution with closed-form solutions in many cases. For the distributed reactive power optimization control model as shown in the following equation:

$$\begin{aligned} &\min \sum_{a=1}^{N} f_a\left(x_a\right) \\ &s.t. \begin{cases} h_a\left(x_a\right) = 0 \\ g_a\left(x_a\right) \ge 0 \end{cases} \end{aligned} \tag{22}$$

Where $f_a(x_a)$ is the objective function of sub-partition a; $h_a(x_a)$ is the equality constraint of sub-partition a; $g_a(x_a)$ is the inequality constraint of sub-partition a; x_a is the subproblem solution for node i in sub-partition a. Region b represents the region adjacent to region a, and $X_{a,ij}$ and $X_{b,ij}$ are the coupling state variables between regions a and b.

The ADMM enables distributed optimal control of partitioned distribution networks. This algorithm performs distributed optimization of reactive power regulation resources across partitions to ensure global optimization. The distributed optimization mechanism between partitions is illustrated in Fig. 1. In this process: Adjacent partitions perform independent optimization calculations in parallel. Each partition adjusts its control variables based on local resources and constraints. Partitions exchange boundary data with neighboring partitions. Boundary variables are updated globally based on the exchanged data. Each partition initiates a new round of local optimization using updated boundary variables. The iterations terminate when the deviation between boundary variables across adjacent partitions falls below a predefined threshold.

Boundary conditions include not only the local optimization results of each partition but also key shared information between adjacent partitions. Define the boundary conditions for adjacent partitions $c_{k\text{-}1}$ and c_k as $B_{c_{k-1}} = \left\{v_i, P_{ij}^*, Q_{ij}^*\right\}$ and $B_{c_k} = \left\{v_i^*, P_{ij}, Q_{ij}\right\}$, respectively. A state variable $\psi_i = \left\{x_i, y_{ij}, z_{ij}\right\}$ is defined to ensure consistency between the boundary conditions of the two partitions, i.e., $B_{c_{k-1}} = \psi_i, \psi_i = B_{c_k}$.

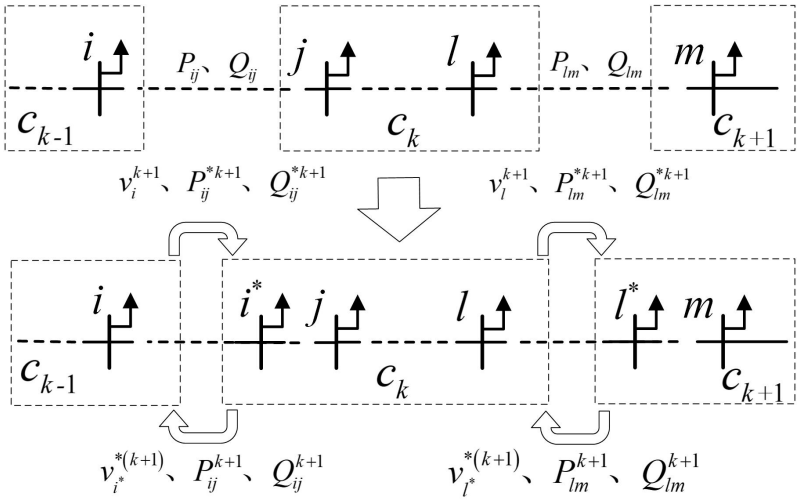

Fig. 1. Schematic diagram of distributed optimal control across partitions

$$\begin{aligned} L_{c_k} = f_{c_k} &+ 0.5\gamma\left\|x_i - v_i^* + \mu_{v_i^*}^t\right\| + 0.5\gamma\left\|y_{ij} - P_{ij} + \mu_{P_{ij}}^t\right\| + 0.5\gamma\left\|z_{ij} - Q_{ij} + \mu_{Q_{ij}}^t\right\| \\ &+ 0.5\gamma\left\|v_l - x_l + \mu_{v_l}^t\right\| + 0.5\gamma\left\|P^*_{lm} - y_{lm} + \mu_{P^*_{lm}}^*\right\| + 0.5\gamma\left\|Q^*_{lm} - z_{lm} + \mu_{Q^*_{lm}}^t\right\| \end{aligned} \tag{23}$$

Detailed Procedure:

(1) Construct the augmented Lagrangian function. Based on the objective function in (10), the augmented Lagrangian function is formulated as (23). In (23), t is the iteration times; γ is the penalty factor, which balances the influence of the objective function and constraints while accelerating algorithm convergence, $\gamma > 0$; $\mu_{v_i^*}^t$ is the voltage at the virtual balancing node i^* of partition c_k; $\mu_{P_{ij}}^t$ and $\mu_{Q_{ij}}^t$ are the active power and reactive power transmitted through line ij between partitions; $\mu_{v_l}^t$ is the voltage at boundary node l; $\mu_{P^*_{lm}}^*$ and $\mu_{Q^*_{lm}}^t$ are the Lagrangian multipliers for the virtual active and reactive loads at boundary node l; x represents the global value of node voltage; y and z are the global values of active and reactive power transmitted through inter-partition lines.

(2) Distributed parallel optimization. Each partition performs independent local optimization using (23) as the objective. Define the optimal solution for node a in partition c_k as $X_{c_k} = \left\{P_{c_k,a}, Q_{c_k,a}, v_{c_k,a}, i_{c_k,a}\right\}$. Set the boundary variables $B_{up} = \left\{v_i^*, P_{ij}, Q_{ij}\right\}$ for all upstream partitions and $B_{down} = \left\{v_l, P^*_{lm}, Q^*_{lm}\right\}$ for downstream partitions.

$$\left\{X_{c_k}^{t+1}, B_{up}^{t+1}, B_{down}^{t+1}\right\} = \arg\min L_{c_k} \tag{24}$$

(3) Boundary data exchange and global variable update. Adjacent partitions exchange boundary data and update global variable values based on the exchanged information. (25) and (26) update the upstream and downstream boundary variables, respectively, ensuring consistency and coordination between neighboring partitions.

$$\begin{cases} x_i^{t+1} = \left(v_i^{t+1} + v_i^{*(t+1)}\right)/2 \\ y_{ij}^{t+1} = \left(P_{ij}^{t+1} + P_{ij}^{*(t+1)}\right)/2 \\ z_{ij}^{t+1} = \left(Q_{ij}^{t+1} + Q_{ij}^{*(t+1)}\right)/2 \end{cases} \tag{25}$$

$$\begin{cases} x_l^{t+1} = \left(v_l^{t+1} + v_l^{*(t+1)}\right)/2 \\ y_{lm}^{t+1} = \left(P_{lm}^{t+1} + P_{lm}^{*(t+1)}\right)/2 \\ z_{lm}^{t+1} = \left(Q_{lm}^{t+1} + Q_{lm}^{*(t+1)}\right)/2 \end{cases} \tag{26}$$

(4) Lagrangian Multiplier Update. Each partition locally updates the Lagrangian multipliers for boundary variables using the received boundary data. (27) and (28) update the Lagrangian multipliers for upstream and downstream boundary variables, respectively.

$$\begin{cases} \mu_{v_i^*}^{t+1} = \mu_{v_i^*}^t + \gamma\left(x_i^{t+1} - v_i^{*(t+1)}\right) \\ \mu_{P_{ij}}^{t+1} = \mu_{P_{ij}}^t + \gamma\left(y_{ij}^{t+1} - P_{ij}^{(t+1)}\right) \\ \mu_{Q_{ij}}^{t+1} = \mu_{Q_{ij}}^t + \gamma\left(z_{ij}^{t+1} - Q_{ij}^{(t+1)}\right) \end{cases} \tag{27}$$

$$\begin{cases} \mu = \mu_{v_l}^t + \gamma\left(v_l^{t+1} - x_l^{t+1}\right) \\ \mu_{P^*_{lm}}^{t+1} = \mu_{P^*_{lm}}^t + \gamma\left(P_{lm}^{*(t+1)} - y_{lm}^{t+1}\right) \\ \mu_{Q^*_{lm}}^{t+1} = \mu_{Q^*_{lm}}^t + \gamma\left(Q_{lm}^{*(t+1)} - z_{lm}^{t+1}\right) \end{cases} \tag{28}$$

(5) Residual Calculation. Each partition computes the primal residual $r_{c_k}^{t+1}$ and dual residual $s_{c_k}^{t+1}$ of inter-partition boundary data.

$$r_{c_k}^{t+1} = \left|B_{up}^{t+1} - X_{ij}^{t+1}\right| + \left|B_{down}^{t+1} - X_{lm}^{t+1}\right| \tag{29}$$

$$s_{c_k}^{t+1} = \left|X_{ij}^{t+1} - X_{ij}^t\right| + \left|X_{lm}^{t+1} - X_{lm}^t\right| \tag{30}$$

Where $X_{ij}^{t+1} = \left\{x_i^{t+1}, y_{ij}^{t+1}, z_{ij}^{t+1}\right\}$, $X_{lm}^{t+1} = \left\{x_l^{t+1}, y_{lm}^{t+1}, z_{lm}^{t+1}\right\}$ is the global value of the partition c_k.

The distributed optimal control flowchart for partition c_k is shown in Fig. 2.

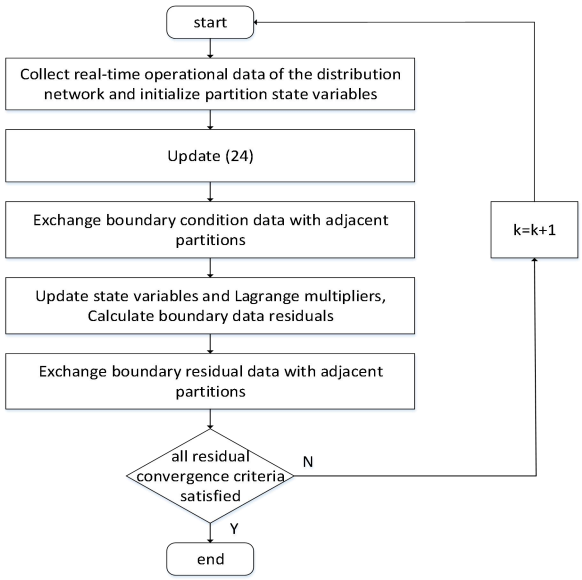

Fig. 2. Distributed optimal control flowchart for partition c_k

The selection of the penalty factor γ in the penalty function has a significant impact on the convergence of the ADMM. Using fixed constants that are either too small or too large can drastically reduce the efficiency of ADMM. Therefore, the value of the penalty factor γ should vary with iterations[20]. This paper proposes an adaptive strategy to adjust the penalty factor, where the adjustment is closely related to the relative magnitudes of the primal residual and dual residual. Under this strategy, the quadratic penalty factor in the augmented Lagrangian function is dynamically updated during iterations to more effectively control the convergence of residuals and accelerate overall algorithm convergence. The specific implementation is as follows:

$$\gamma^{t+1}=\begin{cases}\gamma^t*\left(1+\max\left(R,S\right)/S\right), R>10S\\ \gamma^t/\left(1+\max\left(R,S\right)/S\right), R<10S\\ \gamma^t, others\end{cases} \quad (31)$$

IV. Case Analysis

To verify the effectiveness of the proposed method, the standard IEEE33 node system was modified and simulated in MATLAB. The system's base voltage is 12.66 kV, base capacity is 10 MW, power factor is 0.95, and the allowable voltage violations magnitude range for nodes is [0.95, 1.05] p.u. In the modified IEEE33 node system, 8 distributed PV units and 3 SVC were configured. The installation locations and capacity index of distributed PV and SVC at each node are detailed in Table I.

TABLE I
Access Location and Capacity of Distributed PV and SVC

Controllable Resources	Capacity/kVA	Location
Distributed PV	200	4, 7, 27, 32
	300	10, 17, 20, 24
SVC	100	5, 10, 29

A. Case Analysis on Partitioning of Distribution Networks with Photovoltaic Integration

To accurately evaluate the superiority of the proposed improved modularity index in determining optimal partitioning, the Louvain algorithm was applied to perform partitioning calculations based on both the electrical distance index and the proposed improved modularity index. The modularity index values under both indexes are shown in Table II.

TABLE II
Modurity Index Values under Different Indexs

Method	Modularity Index value	Number of Partitions
Only electrical distance index	0.648	5
Improved modularity index	0.701	3

The stochastic nature of PV installation leads to resource allocation in the network that does not strictly align with structural electrical connectivity. Partitioning based solely on electrical distance may yield suboptimal results. As shown by the modularity function indexes in Table II, for the modified IEEE33 node system, the improved modularity index achieves an 8.18% increase compared to using only the electrical distance index, while reducing the number of partitions from 5 to 3. This demonstrates a more concise network division while maintaining modularity advantages, confirming substantial improvements in partition quality and enhancing overall network performance.

The partitioning results of the modified IEEE33 node system using the electrical distance index and the improved modularity index are shown in Fig. 3. In Fig. 3(a), where only the electrical distance index is applied for distribution network partitioning, partition C4 contains a single node as an isolated partition. By adopting the improved modularity index, such issues are mitigated, preventing partitions with minimal nodes or lacking reactive power resources, thereby eliminating over-centralization or isolated nodes during optimization control.

Furthermore, the improved modularity index achieves more balanced partition sizes and resource distribution. The node count disparity between partitions is significantly reduced, avoiding control complexities caused by excessively large or small partitions. In Fig. 3(a), partitions C1 and C4 exhibit a node count disparity of 11, with partition C4 lacking power quality improvement devices, resulting in reduced flexibility and sustainability. In contrast, Fig. 3(b) demonstrates a maximum node count disparity of 4 under the improved modularity index, ensuring more balanced resource-node configurations across partitions. This enhances grid stability, optimizes control strategies, improves computational efficiency, and strengthens the foundation for subsequent grid dispatching and operational management.

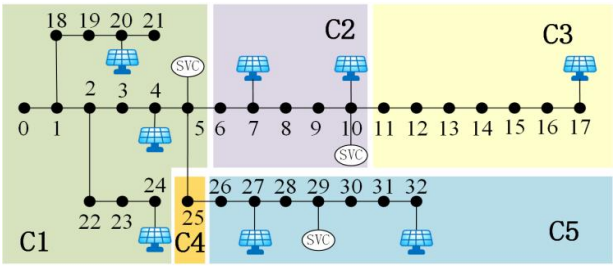

(a) only the electrical distance index

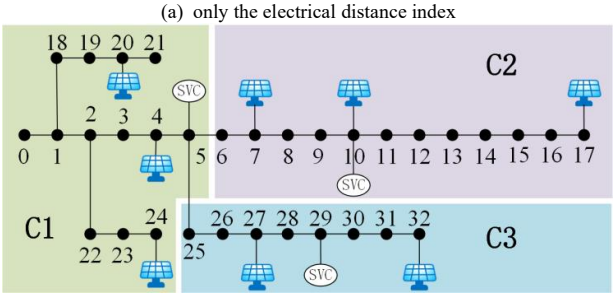

(b) improved modularity index

Fig. 3. IEEE33 node system partition results

The results demonstrate that the improved modularity index not only effectively accounts for electrical distance relationships between clusters but also balances the structural and functional characteristics of the system, achieving more equitable partitioning. This balanced partitioning approach enhances the stability of the distribution network and optimizes its operational efficiency. These findings further validate the practical feasibility of the proposed PV-integrated distribution network partitioning methodology in real-world applications.

B. Case Analysis on Multi-objective Distributed Optimal Control for Photovoltaic-integrated Distribution Networks

To evaluate the effectiveness of the proposed distributed optimization control in mitigating voltage limit violations, reducing network loss, and decreasing inverter losses, the distribution network partitioned using the improved modularity index was optimized and compared with centralized optimization control. This study defines voltage sags caused by remote feeders and large load startups as the primary sources of voltage limit violations. A three-phase short-circuit fault in a remote distribution feeder was simulated, propagating voltage limit violations through the studied PV-integrated distribution network. The voltage violation was simulated at Bus 0 in the network.

Based on the IEEE33 node system partitioned with the improved modularity index, the voltage amplitude curves under centralized and distributed optimization control strategies during a three-phase short-circuit fault are compared in Fig. 4.

When no optimization control is applied, the three-phase short-circuit fault causes voltage sags of varying degrees in all three zones, with the minimum node voltage amplitude dropping to 0.79 p.u. Under centralized optimization control, the voltage amplitudes across all three zones are globally optimized and increased to 0.91 p.u. or higher. With distributed optimization control, the node voltage amplitudes in each zone stabilize above 0.93 p.u., with the overall mean value rising to 0.963 p.u. The standard deviation decreases from 0.063 p.u. to 0.023 p.u., indicating a 61.5% improvement in voltage stability. This demonstrates the accuracy and effectiveness of the distributed optimization scheduling results. Additionally, the voltage amplitude curves under distributed optimization closely match those of centralized optimization, verifying that the proposed distributed control achieves equivalent global optimization effects.

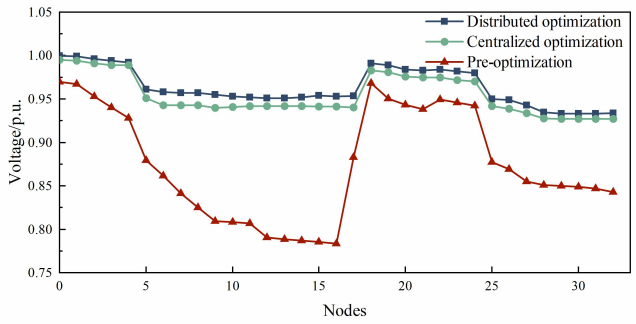

Fig 4. Nodes voltage magnitudes in the IEEE33 node system

When the distributed optimization control strategy converges, the reactive power of distributed PV and SVC in the distribution network is shown in Fig. 5. The coefficient of variation (CV), a standardized indicator for data dispersion defined as the ratio of standard deviation to mean value, measures system equilibrium. The CV for centralized optimization is 0.71, while for distributed optimization it is 0.84. This indicates that centralized control achieves better global equilibrium, but distributed control compensates for this deficiency through localized flexibility. Centralized optimization exhibits excessive reactive power compensation at nodes 7 and 10, potentially inducing unnecessary reactive power flows. In contrast, distributed optimization adjusts reactive power compensation more flexibly and precisely based on actual nodal demands.

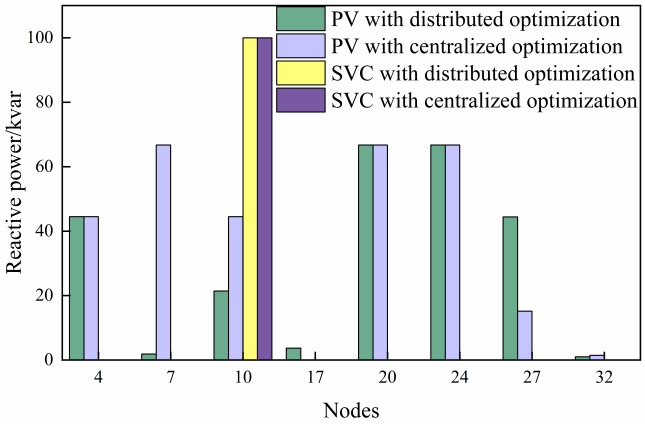

Fig. 5. Reactive power compensation in the IEEE33 node system

A numerical comparison of distributed optimization control and centralized optimization control results is shown in Table III.

TABLE III
REACTIVE POWER COMPENSATION AND NETWORK LOSS UNDER TWO CONTROL STRATEGIES IN THE IEEE33 NODE SYSTEM

Control Method	Reactive Power /kVar	Network Loss and Inverter Loss/kW
Centralized Optimization	406	37
Distributed Optimization	350	18

The distributed optimal control results in a 56 kVar reduction in the total reactive power output of PV systems compared to the centralized optimal control. Additionally, it reduces combined losses in the network and inverters by 19 kW, representing a 51.4% decrease in these losses relative to centralized control. Although both control methods fully utilize system-wide reactive power resources, centralized optimization based on global decision-making may lead to excessive reactive power transmission in certain zones, thereby increasing network loss and inverter loss. These analyses demonstrate that the proposed distributed control achieves global optimization with minimal boundary information exchange. This strategy aligns with the operational characteristics of active distribution networks containing distributed PV, effectively enhancing voltage stability and optimizing grid safety and economic efficiency.

During the iterative process of distributed optimization control, each zone continuously optimizes the reactive power output of its distributed PV systems and SVC. Through information exchange and coordination among clusters, the reactive power allocation gradually converges to a global optimal state. To validate the advantages of the proposed improved ADMM in convergence performance, its residual convergence is compared with traditional ADMM, as shown in Fig. 6 and 7.

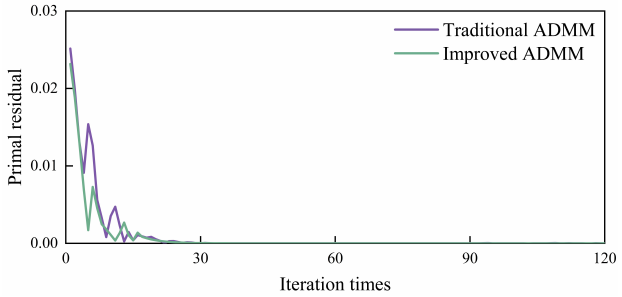

Fig. 6. Boundary primal residuals during distributed optimization control in the IEEE33 node system

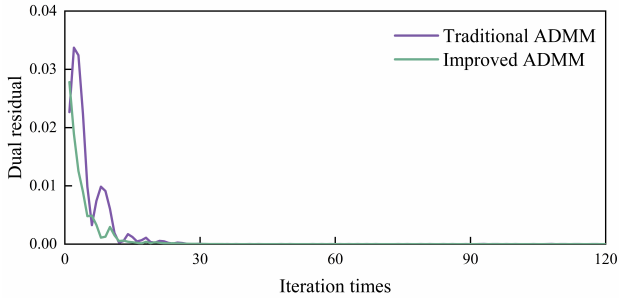

Fig. 7. Boundary dual residuals during distributed optimization control in the IEEE33 node system

The residual convergence curves in Fig. 6 and 7 reveal that traditional ADMM requires 102 iterations to meet the convergence threshold, whereas the improved ADMM achieves the convergence limit in only 45 iterations, significantly reducing computation time.

These results confirm that the improved ADMM outperforms traditional methods in both convergence speed and stability, with a smoother and more efficient residual reduction process.

V. Conclusion

With the increasing penetration of distributed PV systems in distribution networks, rational control of PV-integrated distribution networks is crucial for ensuring their safe, stable, and economical operation. This paper proposes a multi-objective distributed optimization control framework for PV-integrated distribution networks. Case studies and simulation analyses yield the following conclusions:

1) An enhanced electrical distance index, incorporating information from any given node and its neighboring nodes, is introduced. To promote reactive power output and load demand balance within partitioned regions, an intra-region autonomous regulation capability index is formulated. Furthermore, an intra-region coupling strength index is developed to address suboptimal partitioning resulting from the uneven distribution of load nodes and PV access points. These three indices form the basis of a novel, improved modularity index. Validation confirms that this composite index effectively prevents excessive node concentration or isolation during partitioning, ensures equitable resource distribution, and exhibits both theoretical soundness and practical effectiveness.

2) A distributed optimization control model is established post-partitioning, with objectives including minimizing network loss index, voltage violations magnitude, and PV inverter loss index. Simulation results show that the proposed distributed control achieves voltage violation mitigation comparable to centralized optimization methods while reducing computational burden and ensuring grid stability. Furthermore, it reduces network loss index and inverter loss index compared to centralized control and requires less reactive power compensation, thereby improving economic efficiency.

3) To accelerate convergence and enhance optimization performance, an improved ADMM algorithm is proposed. Validation confirms that this method effectively addresses coordinated control challenges in partitioned PV-integrated distribution networks, significantly reduces iteration counts, and improves computational efficiency and solution speed.

References

[1] J. CAO, Y.L. JIN, T. ZHENG, J.J. XU, Y.Q. SI, “A decentralized robust voltage control method for distribution networks considering the uncertainty of distributed generation clusters,” Power System Protection and Control, 2023,51(22):155-166.

[2] L. Ma, J.H. Lou, Y. Li, Y.Y. Chen, X. Liu, Y.H. Zhang, “Severity Assessment of Nonrectangular Wave Voltage Sags from Load Side and Power Side Based on Curve Fitting,” IAENG International Journal of Computer Science, vol. 51, no.10, pp1596-1603, 2024

[3] Reguieg Z, Bouyakoub I, Mehedi F, “Integrated optimization of power quality and energy management in a photovoltaic-battery microgrid,” Renewable Energy, 2025,241:122358-122358.

[4] X.Q. JI, L.H. ZHANG, Q. LIU, et al. “Multi-stage distributed voltage control for flexible interconnected distribution networks considering active and reactive power coordination,” Distribution & Utilization, 2025,42(2):1-11.

[5] J.W. Li, X.Y. Wang, Y.G. Li, X.S. Shi, W. Sun, “Enhancing voltage quality of distribution network with PV power generation system,” ACTA ENERGIAE SOLARIS SINICA, 2018,39(08):2293-2304.

[6] Chen Y, Zhao J, Wan K, et al, “Delay-tolerant hierarchical distributed control for DC microgrid clusters considering microgrid autonomy,” Applied Energy, 2025, 378(PB): 124905-124905.

[7] Q. ZHANG, J.J. DING, D.N. ZHANG, Q.J. WANG, J.H. MA, “Reactive power optimization of high-penetration distributed generation system based on clusters partition,” Automation of Electric

Power Systems, 2019,43(3):130-137.
[8] P.C. ZHENG, Y.H. ZHOU, X.X. CHEN, T.Y. ZHANG, "Active distribution network voltage distributed control strategy based on improved modularization index," Modern Electronics Technique, 2024,47(12):138-144.
[9] Y. Ji, D.D. Yang, Z.D. Zhou, et al, "Voltage coordinated control of distribution network with high proportion distribution photovoltaic considering network partition," Renewable Energy Resources, 2024,42(10):1399-1407.
[10] Vinothkumar K, Selvan M P, "Hierarchical Agglomerative Clustering Algorithm method for distributed generation planning," International Journal of Electrical Power & Energy Systems, 2014, 56:259-269.
[11] L.Z.C. Meng, X.Y. Yang, J. Zhu, X.Z. Wang, X. Meng, "Network partition and distributed voltage coordination control strategy of active distribution network system considering photovoltaic uncertainty," Applied Energy, 2024, 362, 122846-.
[12] B. Zhao, Z. Xu, C. Xu, C.S. Wang, F. Lin, Network Partition-Based Zonal Voltage Control for Distribution Networks With Distributed PV Systems, IEEE Trans Smart Grid, 2018,9(5):4087-4098.
[13] J. Li, Y. Zhang, C. Chen, et al, "Two-Stage Planning of Distributed Power Supply and Energy Storage Capacity Considering Hierarchical Partition Control of Distribution Network with Source-Load-Storage," Energy Engineering, 2024, 121(9):2389-2408.
[14] Y.X. Dong, "Evaluation method of voltage sag severity in distribution networks," International Journal of Energy and Power Engineering, 2021,10(6):135-140.
[15] Y. XU, X.W. YAN, "Dynamic Partitioning Real-Time Reactive Power Optimization Method for Distribution Network with Renewable Distributed Generators Participating in Regulation," Modern Electric Power, 2020,37(01):42-51.
[16] C.J. CHEN, X.L. LI, K.H. JI, Y. WANG, S.F. LIN, "Distribution Network Cluster Partition and Optimal Operation Considering Source-Load-Storage Matching," Electric Power Construction, 2023,44(9):80-93.
[17] H.Z. Xu, X.Y. Mo, H. Li, "Research and discussion on improved louvain algorithm for complex network," Cyberspace Security, 2024,15(01):136-141.
[18] T. Xu, W. Wu, "Accelerated ADMM-Based Fully Distributed Inverter-Based Volt/Var Control Strategy for Active Distribution Networks," IEEE Transactions on Industrial Informatics, 2020, 16(12): 7532-7543.
[19] D.R. Han, "A Survey on Some Recent Developments of Alternating Direction Method of Multipliers," J Oper Res Soc, 2022, 10(1): 1-52.
[20] B. WANG, J.J. MU, X.P. JIAO, Z.F. WANG, "ADMM Penalized Decoding with Layered Scheduling for LDPC Codes Based on Improved Penalty Function," ACTA ELECTRONICA SINICA, 2020,48(04):827-832